PCCP

Accepted Manuscript

ROYAL SOCIETY OF CHEMISTRY

www.rsc.org/pccp

PCCP

RSCPublishing

PAPER

Thermoelectric transport properties of pristine and Na-doped $SnSe_{1-x}Te_x$ polycrystals†

Cite this: DOI: 10.1039/x0xx00000x

Tian-Ran Wei, Chao-Feng Wu, Xiaozhi Zhang, Qing Tan, Li Sun, Yu Pan and Jing-Feng Li*

Received ooth January 2012,
Accepted ooth January 2012

DOI: 10.1039/x0xx00000x

www.rsc.org/

SnSe, a "simple" and "old" binary compound composed of earth-abundant elements, has been reported to exhibit a high thermoelectric performance in single crystals, which stimulated recent interests in its polycrystalline counterparts. This work investigated the electrical and thermal transport properties of pristine and Na-doped $SnSe_{1-x}Te_x$ polycrystals prepared by mechanical alloying and spark plasma sintering. It is revealed that $SnSe_{1-x}Te_x$ solid solutions are formed when x ranges from 0 to 0.2. An energy barrier scattering mechanism is suitable for understanding the electrical conducting behaviour observed in the present SnSe polycrystalline materials, which may be associated with abundant defects at grain boundaries. The thermal conductivity was greatly reduced upon Te substitution due to alloy scattering of phonons as well explained by Debye model. Due to the increased carrier concentration by Na-doping, thermoelectric figure of merit (*ZT*) was enhanced in the whole temperature range with a maximum value of 0.72 obtained at a relatively low temperature (773 K) for $Sn_{0.99}Na_{0.01}Se_{0.84}Te_{0.16}$.

1. Introduction

Thermoelectric (TE) materials and technologies that are capable of directly converting waste heat into electricity can offer an additional solution to the current concerns on carbon-based fuel consumption and greenhouse gas emissions.[1,2] For decades, it has been the common goal for the thermoelectric community to develop promising materials with a high dimensionless figure of merit *ZT* (defined as $ZT=S^2T/\rho\kappa$, where *S*, *T*, ρ and κ are Seebeck coefficient, absolute temperature, electrical resistivity and thermal conductivity, respectively).[3-6] It is of no less importance at the same time, however, to explore TE materials free of the toxic Pb based on environmental concerns. Various compounds have been discovered to exhibit promising *ZT* values comparable to the commercially used PbTe-[7] and Bi_2Te_3-based[8] materials, such as skutterudites,[9] Half-Heusler compounds[10] and Mg_2X (X=Si, Ge, Sn).[11]

Recently, the "simple" and "old" binary compound SnSe containing earth-abundant elements was reported to possess an extraordinarily high *ZT*~2.6 (at 923 K) along *b*-axis in its single crystal form,[12] benefiting mainly from the intrinsically low thermal conductivity that was ascribed to the large lattice anharmonicity.[12,13] Since then attention has also been paid to polycrystalline SnSe of both p-[14,15] and n-types[16] considering their better machinability and prospect of large-scale applications, but the reported *ZT* values are much lower than single crystals. It is thus highly desired to enhance thermoelectric performance of the polycrystalline counterparts. This goal, however, should be accomplished based on an in-depth understanding of the electrical and thermal transport properties which are likely to differ from those of single crystals.

Chemical doping is widely employed to tune the carrier concentration and improve *ZT* of thermoelectrics. In addition, alloying is one of the most effective ways to reduce thermal conductivity of TE materials (such as lead chalcogenides,[17,18] Bi_2Te_3-based alloys[19] and diamond-like copper chalcogenides[20]), and even to optimize electrical transport properties by virtue of band engineering.[21,22] In fact, SnSe has been found to form complete solid solutions with SnS, an isostructural binary chalcogenide,[23] and exhibit reduced thermal conductivities as well as enhanced *ZT* values.[16,24] Being different from SnS and SnSe, the homologous compound SnTe crystallizes in a NaCl-like, cubic structure featured with high band degeneracies, small band gap, semi-metallic transport behaviour[25] and promising TE performance.[26] It is thus expected that by substituting Te for Se, interesting variations in transport properties and possible performance enhancement will be found. Nonetheless, relevant reports on this issue are severely inadequate. Chen *et al.*[27] studied experimentally and theoretically the effect of Te doping on SnSe, but the amount of Te was limited to 0 and

0.0625, and all the samples exhibited a surprisingly n-type conduction behaviour.

The present work was conducted focusing on pristine and Na-doped $SnSe_{1-x}Te_x$ alloys with two motivations; one is to reveal the electrical and thermal transport mechanisms in polycrystalline SnSe, and the other is to enhance the thermoelectric performance of the polycrystals by doping and alloying. The carrier transport behaviour was found to obey a barrier scattering mechanism rather than that reported previously.[12,14] Te-substitution greatly reduced the thermal conductivity and band gap of SnSe, and the thermal transport property was well modelled on the basis of point defect scattering of phonons. By doping with Na, the carrier concentration and electrical conductivity were greatly enhanced, leading to a maximum *ZT* of 0.72 at a relatively low temperature (773 K).

2. Experimental

Polycrystalline samples were fabricated by spark plasma sintering (SPS) of the powders that were pre-synthesized by mechanical alloying (MA). Sn (99.99%), Se (99.9%) and Te (99.99%) powders and Na pieces (99.5%) were weighed according to the stoichiometry of $SnSe_{1-x}Te_x$ and $Sn_{0.99}Na_{0.01}Se_{1-x}Te_x$ (x=0-0.28), and milled on a planetary ball mill at 450 rpm for 15 h using a stainless steel vessel filled with a mixed atmosphere of 95 vol% Ar and 5 vol% H_2 gases. The MA-processed powders were loaded into a graphite die and then sintered by SPS (SPS-211Lx, Fuji Electronic Industrial, Japan) at 793 K for 5 min under a uniaxial pressure of 50 MPa, yielding a cylinder-shaped sample with ~8 mm in height and ~15 mm in diameter. Note that powder handling was done in a glove box filled with Ar.

The phase structures were investigated by using X-ray diffraction (XRD, D/Max 2500, Rigaku, Japan) with Cu K_α radiation. Scanning electron microscopy (SEM) images of the bulk materials were taken in the secondary electron (SE2) and backscattering electron (BSE) detector modes using a field emission scanning electron microscope (FE-SEM, JSM-7001, JEOL, Japan). Microstructure and selected area electron diffraction (SAED) pattern were observed by a transmission electron microscope (TEM, JEM-2100, JEOL, Japan). Electronic probe microscopic analysis (EPMA, JXA-8230, JEOL, Japan) was carried out to map elemental distribution on polished surface of bulk samples. Seebeck coefficient (*S*) and electrical resistivity (ρ) measurement was conducted on a bar-shaped specimen by using a Seebeck coefficient/electric resistance measuring system (ZEM-2, Ulvac-Riko, Japan). Hall coefficient (R_H) was measured under a reversible magnetic field by the Van der Pauw technique using a Hall measurement system (ResiTest 8340DC, Toyo, Japan). Hall carrier density (n_H) was calculated *via* $n_H=1/(eR_H)$, and Hall carrier mobility (μ_H) was obtained through $\mu_H=R_H/\rho$. The thermal diffusivity (*D*) was measured by using a laser flash diffusivity method (TC9000, Ulvac-Riko, Japan). The specific heat capacity (C_P) was taken from ref. 12 for SnSe and estimated based on linear relationships for Te-substituted samples where C_P for SnTe was given in ref. 25. For Na-doped samples, C_p was taken equal to undoped ones considering the small amount of the dopant. Thermal conductivity (κ) was calculated by $\kappa=DC_Pd$, where *d* is the density measured by the Archimedes method. Considering the layered structure and anisotropy (see Fig. S1 in ESI†) of SnSe, both the electrical and thermal transport properties were measured in the same direction that is perpendicular to the pressure during SPS. According to Ortiz *et al*., transport in this direction can be regarded as that in randomly oriented polycrystals as supported by continuous Debye rings.[28] Optical absorption measurements were conducted on powders by using the UV-Vis-NIR spectrum system (Cary 5000, Varian, USA) at room temperature (RT). The indirect gaps were obtained by extrapolating $(\alpha hv)^{1/2}$ to 0 as a function of hv, where α is the absorption coefficient, hv is the photon energy.

3. Results and discussion

3.1 Solid solution and microstructure

Fig. 1 (a) shows the XRD patterns of $SnSe_{1-x}Te_x$ bulk samples. All the main peaks were indexed to the orthorhombic phase with *Pnma* symmetry (PDF #48-1224) without secondary phases being found within the detection limit. The peaks shift towards lower angle values with increasing amount of Te, indicating enlarged lattice parameters. As shown in Fig. 1 (b), the lattice cell volume exhibits a linear increase with x in the range of 0-0.2, being consistent with ref. 28. It is noticed that for the samples with higher amounts of Te (x = 0.24 and 0.28), some peaks tend to diminish, suggesting increased degree of crystal symmetry. Based on the XRD results, it is speculated that $SnSe_{1-x}Te_x$ solid solutions are formed when x varied from 0 to 0.2 which is within the solubility.[28,29]

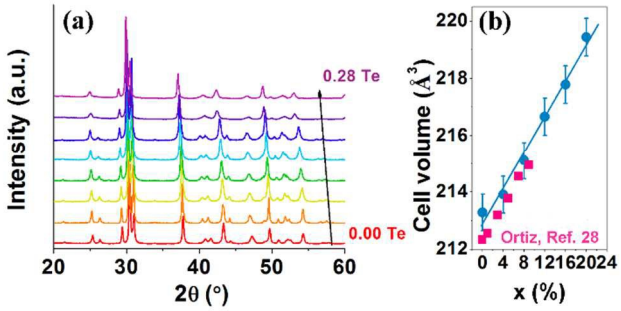

Fig. 1 (a) XRD patterns of $SnSe_{1-x}Te_x$ (x=0-0.28) and (b) cell volume as a function of Te content together with the data (pink squares) from ref. 28 as a comparison.

Alloying effect was also confirmed by the composition-dependent optical absorption spectra and band gap as shown in Fig. 2. A clear absorption edge around 0.9 eV is seen for SnSe, and the curves demonstrate a red-shift upon Te substitution. As depicted in the inset panel, E_g of pristine SnSe in this work is ~0.85 eV and is well consistent with previously reported values.[12,16] E_g keeps decreasing to about 0.6 eV and seems to saturate when x reaches 0.16.

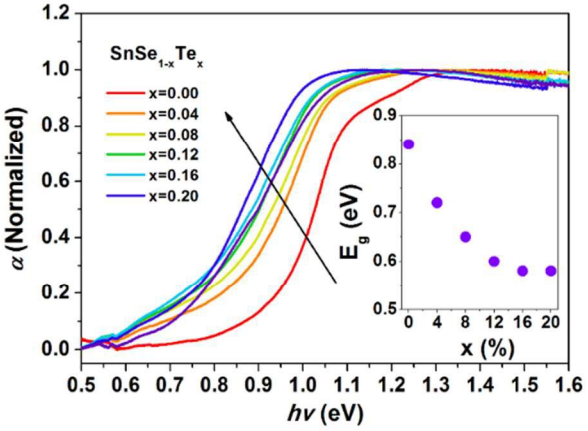

Fig. 2 Optical absorption spectra of $SnSe_{1-x}Te_x$ (x=0-0.2) powders. The inset shows the calculated indirect band gaps of the compounds.

SnSe exhibits a dense microstructure composed of lamellar grains with the width of 100-200 nm as shown in Fig. 3 (a) and (d). The grain boundaries, manifested in Fig. 3 (e), are clean and clear, suggesting good crystallinity and high quality of the samples prepared by MA and SPS. The SAED pattern in Fig. 3 (f) was indexed as SnSe of *Pnma* space group with no spots corresponding to other phases or sublattices. Upon Te alloying, the grains become larger [see Fig. 3 (a)-(c)], possibly due to the lower melting points of solid solutions than pure SnSe.[29] In addition, more voids are observed in $SnSe_{1-x}Te_x$ which are also demonstrated by the polished surface morphology in Fig. 4 (b). In fact, SnSe has a porosity < 4% while the value is noticeably larger for Te-substituted samples (8-11%). It seems that Se volatilization is more notable in $SnSe_{1-x}Te_x$ (the weight losses of Se derived from EPMA data are 0.05, 0.07 and 0.11 for SnSe, $SnSe_{0.92}Te_{0.08}$ and $SnSe_{0.84}Te_{0.16}$, respectively), leaving small and scattered voids in the matrix. As shown by the

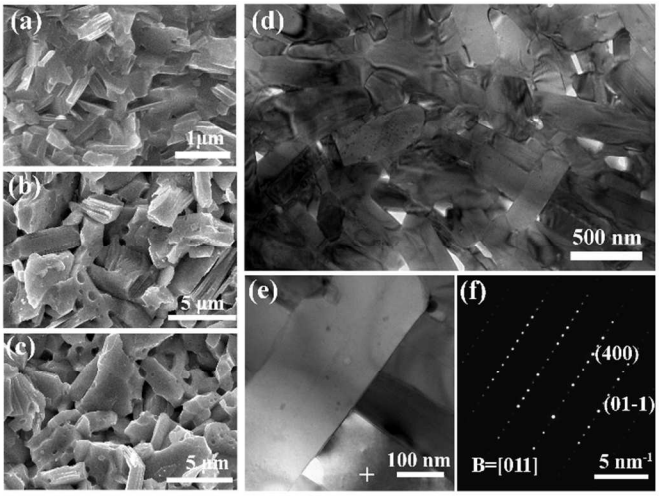

Fig. 3 (a)-(c) Fractured surface morphologies of $SnSe_{1-x}Te_x$ (x=0, 0.08 and 0.20); (d), (e) TEM images and (f) SAED pattern taken in the grain marked by "+" in (e) for SnSe.

EPMA mapping profile in Fig. 4, Sn and Se are found to uniformly distribute in both SnSe and $SnSe_{1-x}Te_x$ while small inhomogeneity of Te distribution is seen in solid solutions which may be caused by the low diffusivity of this large and heavy element.

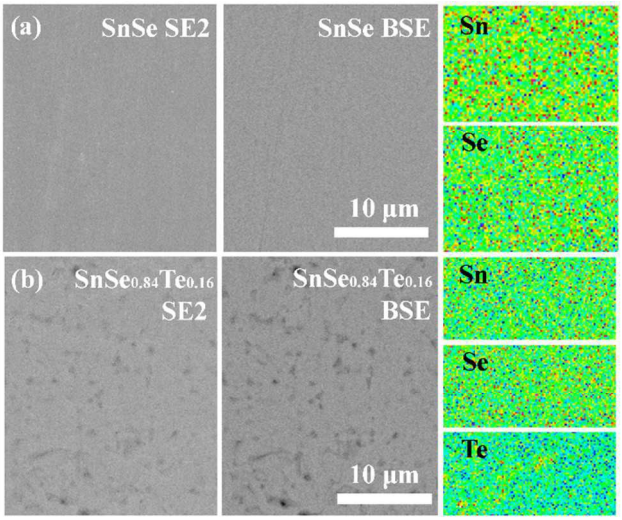

Fig. 4 Polished surface morphology in secondary electron (SE2), back scattering electron (BSE) modes and elemental distribution by EPMA mapping for (a) SnSe and (b) $SnSe_{0.84}Te_{0.16}$.

3.2 Electrical transport properties

Undoped $SnSe_{1-x}Te_x$ exhibit relatively high resistivity (ρ) and Seebeck coefficient (S) as shown in Fig. 5 (a) and (b), respectively. For pristine SnSe, ρ keeps decreasing with temperature while S exhibits somewhat a metallic behaviour. The rollover of S around 650 K indicates the onset of excitation of minority carriers.[30] Transport behaviours of Te-substituted samples seem out of expectation; with a narrower band gap by incorporating Te into the lattice, the electrical resistivity is larger than that of the pristine SnSe, resulting in lower power factors (*PF*s). However, when doped with 1 mol% Na, the electrical resistivity of $SnSe_{1-x}Te_x$ samples greatly decreased from 10-100 Ω.cm to 10-100 mΩ.cm at RT [Fig. 5 (d)]. S is also smaller for doped samples. For all the Na-doped samples, ρ firstly decreases with T, then turns to increase at ~550 K but finally decreases at T > ~650 K. Anomaly in electrical transport around 500 K was also found in ref. 15 and was tentatively ascribed to the melting of very small amount of unreacted Sn.[15,16] In this work, however, no phase transition is indicated in the Differential Scanning Calorimetry (DSC) patterns between 400 and 600 K (see Fig. S2 in ESI†). Such non-monotonic variations in ρ and S with T should be further understood with an insight into carrier concentration and mobility.

As shown in Fig. 6 (a), the Hall carrier concentration n_H is relatively high (~7×10^{17} cm^{-3}) for undoped SnSe prepared by MA and SPS in this work, and shows a relatively weak temperature dependence from RT up to ~623 K. At higher temperatures, n_H increases rapidly with T, indicating intrinsic excitations which were also reflected in temperature-dependent Seebeck coefficient [Fig. 5

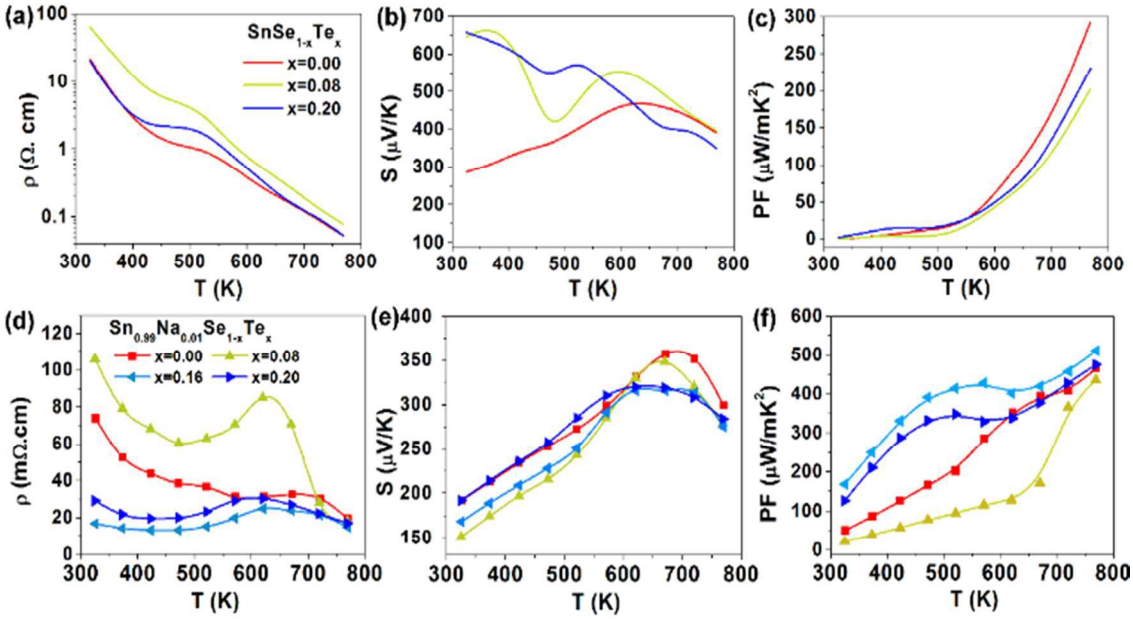

Fig. 5 Temperature-dependent electrical properties for $SnSe_{1-x}Te_x$ [(a)-(c)] and $Sn_{0.99}Na_{0.01}Se_{1-x}Te_x$ [(d)-(f)].

(b)]. The fact that n_H is higher in this work than that in ref. 12 and 14 (~2×10^{17} cm^{-3}) is probably related to specific crystal defects, possibly Sn vacancies, which act as shallow acceptors and were probably generated during ball milling[31] and maintained in the SPS process. In fact, in some other TE materials, such as BiCuSeO,[32] Sb_2Te_3 (ref. 33) and Bi_2Te_3-based compounds,[34-36] ball milling was found to introduce appreciable defects and reasonably change the carrier concentration. When doped with Na, n_H increases to ~1×10^{19} cm^{-3} at RT and shows even weaker temperature dependence. Bipolar effect is also seen in the doped sample around 650 K, but the rise is not as sharp as that in the undoped one due to the suppression by higher majority carrier concentration.

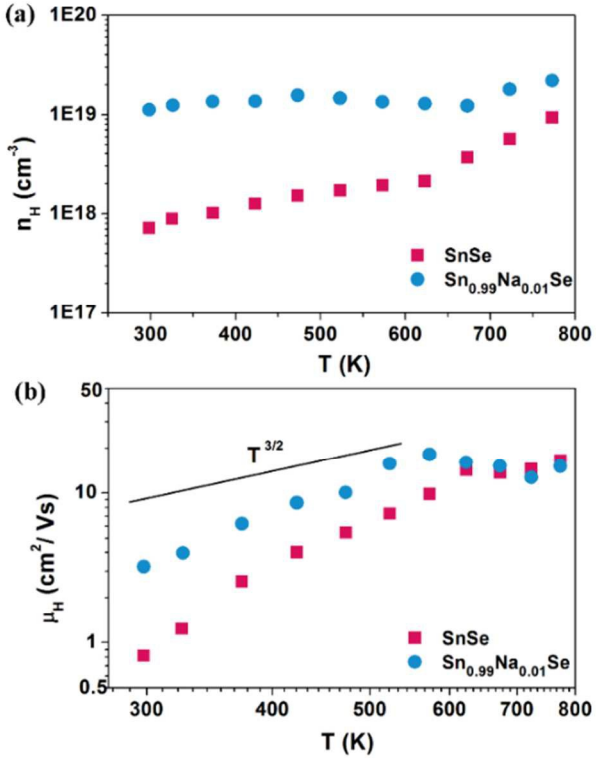

Fig. 6 (a) Hall carrier concentration and (b) Hall mobility varying with temperature for SnSe and $Sn_{0.99}Na_{0.01}Se$.

For both undoped and doped samples, as shown in Fig. 6 (b), μ_H increases from RT to ~550 K. It is noted here that: (1) μ_H cannot be described by a simple power law with temperature corresponding to a certain scattering mechanism; (2) with a higher n_H, Na-doped sample shows a higher mobility than the undoped one. The behaviours of mobility here are different from most of the well-known TE materials where acoustic phonon scattering dominates. This phenomenon was ascribed to an energy barrier scattering process and will be discussed later.

Now the temperature dependence of resistivity in Fig. 5 (a) and (d) can be well understood. At low temperatures μ_H increases rapidly with temperature while n_H keeps roughly unchanged, bringing about obvious reduction in ρ. When T rises to ~550 K, n_H still shows a weak T-dependence, but μ_H starts to decrease, so ρ turns to increase with T. At T > ~650 K, intrinsic excitation takes place, causing an increase in n_H while μ_H decreases just slightly, thus leading to the final reduction in ρ.

Here we refocus on the carrier mobility shown in Fig. 6 (b). For most of the well-known thermoelectric materials, carriers are mainly scattered by long-wave acoustic phonons, showing the temperature dependence of $\mu \propto T^{-3/2}$ (ref. 30 and 37). In addition, ionized impurity scattering is also expected in some semiconductors with the

relationship of $\mu \propto T^{3/2}$ (ref. 30). Nonetheless the T-dependence of μ_H in this work could not be explained by a certain scattering mechanism. Particularly, at low temperatures μ_H rises even faster than what is predicted by ionized impurity scattering that has the largest power among the common scattering mechanisms for thermoelectrics. A rapid increase of mobility is often a suggestion of a hopping process or an energy barrier scattering,[38] and a similar behaviour was also observed in the isostructural SnS prepared by the same method.[39] Here we referred to a grain boundary barrier scattering mechanism to describe the mobility. This model was proposed to explain the charge transport in polycrystalline silicon films[40] and later was well applied to some TE materials.[41-43]

MA-synthesized powders tend to have high chemical reactivity due to the refined grains and accumulated energy brought by high-energy ball milling.[31] As a result, chemisorption of oxygen or generation of crystal defects is expected, which is likely to result in increased trapping of carriers at grain boundaries, thus forming energy barriers that impede the motion of carriers from one grain to another. Assuming a uniformly distributed concentration of ionized carrier traps and barrier, and a grain-boundary thickness that is much less than the crystallite size L, the effective mobility is given by

$$\mu = Le\left(\frac{1}{2\pi m^* k_B T}\right)^{1/2} \exp\left(-\frac{E_B}{k_B T}\right) \quad (1)$$

where m^* is the effective mass of carriers, E_B is the energy barrier height.[40,41] As shown in Fig. 7, a clearly linear relationship is seen between ln ($\mu T^{1/2}$) and $(k_B T)^{-1}$ yielding E_B = 169 and 129 meV for pristine and Na-doped SnSe, respectively. The doped sample was found to have a higher mobility and a lower barrier height than the undoped one. This is because for the doped sample with a larger carrier density, the chemical potential is deeper in the valence band; in other words, hole carriers have a higher average energy to get rid of the trap of defects at grain boundaries, thus showing a lower barrier height and a higher mobility.

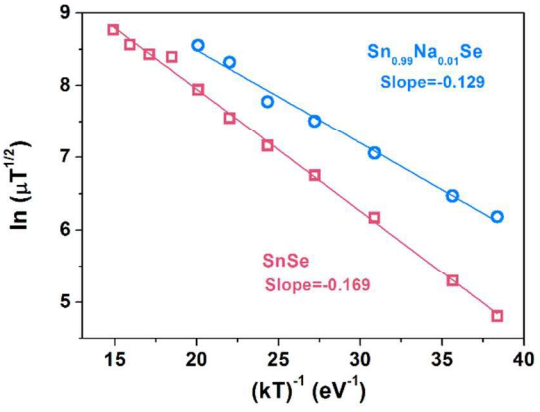

Fig. 7 Energy barrier scattering in pristine and Na-doped SnSe prepared by MA and SPS

It should be mentioned here that the value of Hall mobility μ_H is not exactly equal to the drift mobility μ_d or the "effective" mobility μ in the above equation taking into account the influence of Fermi level and scattering mechanism. Usually a pre-factor r_H is used to link μ_H and μ_d, and this factor is often calculated within the framework of single parabolic band (SPB)[37] or Kane band (SKB)[44,45] approximations. Here, however, considering the barrier scattering mechanism in SnSe, neither SPB nor SKB seems appropriate for modelling charge transport, so we used μ_H as the effective mobility in Eqn. (1) with an estimated error of 10-15% that is comparable to that of the Hall measurements.

3.3 Thermal transport and thermoelectric properties

Thermal conductivities as a function of temperature for $SnSe_{1-x}Te_x$ are shown in Fig. 8 (a). Generally κ decreases with temperature and Te content, suggesting enhanced Umklapp and alloy scattering of phonons, respectively. For the x=0.24 sample, κ rises obviously at high temperatures, which is a clear indication of bipolar effect. By comparing Fig. 8 (a) and (b) it is seen that Na-doped samples exhibit slightly higher κ than undoped ones with the same amount of Te, which is due to the increased electronic thermal conductivity.

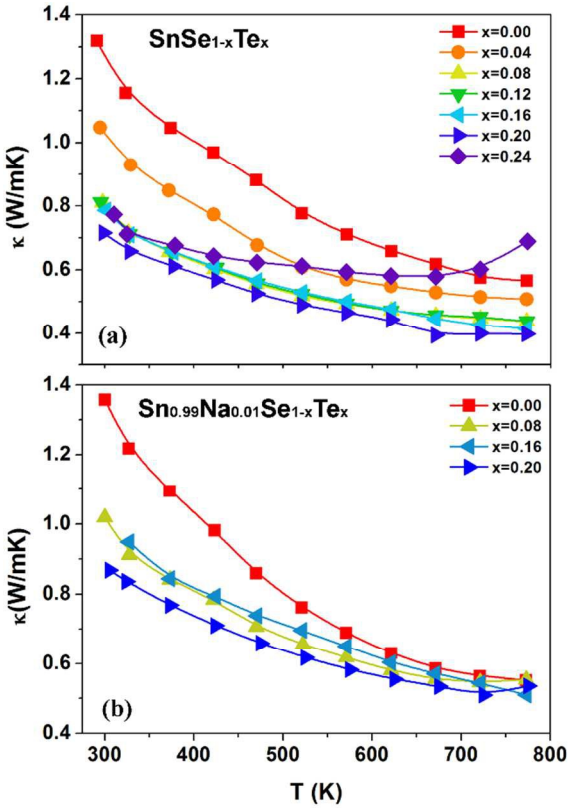

Fig. 8 Thermal conductivities as a function of temperature for (a) $SnSe_{1-x}Te_x$ and (b) $Sn_{0.99}Na_{0.01}Se_{1-x}Te_x$.

In order to further understand the role of Te alloying in thermal transport of SnSe, we modelled the data within Debye approximation. For analyzing the thermal transport properties of all the samples with different densities, thermal conductivity of $SnSe_{1-x}Te_x$ without Na-doping was corrected to 100% dense samples to exclude the effect of porosity *via*:

$$\frac{\kappa_{real}}{\kappa_{dense}} = 1 - \frac{4}{3}\phi \quad (2)$$

where κ_{real} is the measured value of our samples, κ_{dense} corresponds to that of fully dense ones, and ϕ is the porosity.[46] For the undoped $SnSe_{1-x}Te_x$ alloys, the electrical conductivity is rather low [Fig. 5(a)], so here the lattice thermal conductivity was treated numerally equal to the total one.

In the framework of Debye model, the lattice thermal conductivity can be treated as the cumulative contribution of phonons varying in frequency from 0 to the upper limit *via*[47,48]

$$\kappa_L = \frac{k_B}{2\pi^2 v}\left(\frac{k_B T}{\hbar}\right)^3 \int_0^{\theta_a/T} \tau(x)\frac{e^x x^4}{\left(e^x-1\right)^2}dx, \quad (3)$$

where v is the average sound speed, θ_a is the average acoustic Debye temperature, $x = \hbar\omega / k_B T$ is the reduced phonon energy, and $\tau(x)$ is the total relaxation time. Since it has been mentioned above that transport in the direction perpendicular to pressure is expected to be consistent with randomly oriented polycrystalline samples,[28] we calculated v from the values for each axis in ref. 12 *via* $v^{-3} = \left(v_a^{-3} + v_b^{-3} + v_c^{-3}\right)/3$. It is interesting to note that this value (1674 m/s) is well consistent with the measured one (~1560 m/s) in ref. 28. θ_a was calculated from the Debye temperature Θ (a commonly used value derived from heat capacity or elastic properties) *via* $\theta_a = \Theta / n^{1/3}$,(ref. 49) where n=8 for SnSe is the atomic number per primitive unit cell and Θ = 215 K was taken from ref. 50-52.

The total relaxation time is determined by various scattering processes:

$$\tau^{-1} = \tau_U^{-1} + \tau_{GB}^{-1} + \tau_{PD}^{-1}. \quad (4)$$

Here the footnotes U, GB and PD denote Umklapp, grain boundary and point defect scattering, respectively. In this work, the Normal (N) process[53] of phonon scattering was not taken into account for its limited role when there exist appreciable amount of defects.[48] Each scattering process is dependent on temperature and/or phonons' frequency (energy). For Umklapp process, the scattering frequency is given by[54]

$$\tau_U^{-1}(x) = \frac{k_B{}^2\gamma^2}{\hbar M v^2 \theta_a} x^2 T^3 e^{-\theta_a/3T} \quad (5)$$

where M is the average mass per atom, and γ is the Grüneisen parameter characterizing the lattice and bond anharmonicity. For grain boundary scattering, the relaxation time of phonons is limited by the grain size L *via*:

$$\tau_{GB}^{-1}(x) = v / \mathrm{L} \quad (6)$$

The point defects dominant scattering is associated with the parameter Γ *via*[55]

$$\tau_{PD}^{-1}(x) = \frac{k_B{}^4 V_{atom}\Gamma}{4\pi\hbar^4 v^3} x^4 T^4 \quad (7)$$

Here $\Gamma = \Gamma_{mass} + \Gamma_{strain}$ quantifies the fluctuations in mass and strain caused by impurity atoms. For the case of only two atoms on one sublattice, the two terms can be expressed as:[56]

$$\Gamma_{mass} = n_{sublatt}\left(\frac{\overline{M_{sublatt}}}{\overline{M_{compd}}}\right)^2 f_1 f_2 \left[\frac{M_1 - M_2}{\overline{M_{sublatt}}}\right]^2 / n_{compd} \quad (8)$$

$$\Gamma_{strain} = n_{sublatt}\left(\frac{\overline{M_{sublatt}}}{\overline{M_{compd}}}\right)^2 f_1 f_2 \varepsilon \left[\frac{R_1 - R_2}{\overline{R_{sublatt}}}\right]^2 / n_{compd} \quad (9)$$

where n_{sublatt}, $\overline{M_{sublatt}}$ and $\overline{R_{sublatt}}$ are the occupancy, average atomic mass and average atomic radius of the sublattice; f_i, M_i and R_i (i=1, 2) are the occupational fraction, atomic mass and radius (taken from ref. 57) of atoms 1 and 2, respectively; n_{compd} and M_{compd} are the total occupancy and average atomic mass of all the sublattices of the compound. Here for $SnSe_{1-x}Te_x$, n_{sublatt}=1 and n_{compd}=2. ε is a phenomenological adjustable parameter that is related to elastic properties.[20,58]

For pristine SnSe, we neglected point defect scattering, and then the only undetermined parameter is γ. By fitting the experimental data for SnSe from 300 to 773 K, we found γ = 2.65 yielded the best simulation and this value is very close to that (2.98) in ref. 50. For $SnSe_{1-x}Te_x$, the values of θ_a, v, γ and L were set equal to those of SnSe based on the following considerations: (1) Te content (x) is relatively low in this work, so large deviations in these parameters are not expected upon Te substitution; (2) different models or treatments can yield various fitting values. Although a linear average is a good approximation for complete solid solutions such as lead chalcogenides,[17] it is not quite reasonable for $SnSe_{1-x}Te_x$ considering the difference in crystal structure of the binary compounds and the limited solubility of Te in SnSe. Then ε = 135 was determined by fitting thermal conductivity versus Te content at 300 K, which seems to go beyond the common range of 10-100,[56] but is still a reasonable value when compared with lead chalcogenide alloys (100-150),[17] Cu_3SbSe_4- (136, 190),[20,58] and ZrNiSn-based[56] solid solutions. The parameters used for modelling are listed in Table 1.

Table 1 Parameters for thermal transport modeling

Parameter (unit)[a]	Value	Notes and references
Debye temperature, θ_a (K)	107.5	ref. 50-52
Sound speed, v (m/s)	1674	ref. 12
Grüneisen parameter, γ	2.65	Fitted
Grain size, L (μm)	2[b]	--
Adjustable parameter, ε	135	Fitted

[a] θ_a, v and γ here refer to average parameters for acoustic branches.
[b] It is difficult to obtain accurate grain size for layered compounds. Nonetheless we found that by changing L from 500 nm to 2 μm, the resultant thermal conductivity varies within only 5 % at 300 K.

Corrected thermal conductivities and modelling results as functions of temperature and Te content are shown in Fig. 9 (a) and (b), respectively. It is seen that the modelling results can well fit the experimental ones, especially at T < 600 K where bipolar effect is not obvious. As shown in Fig. 9 (b), 30-40% reduction in thermal conductivity at RT was captured by calculation when x increases from 0 to 0.2. The inset further demonstrates that strain field fluctuation plays a dominant role in point defect scattering of phonons, which is caused by the ionic size difference between Se and Te.

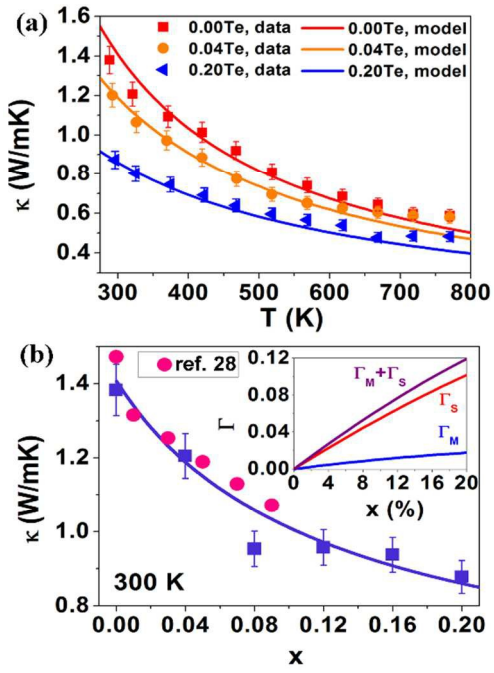

Fig. 9 Corrected thermal conductivities as functions of (a) temperature and (b) Te content together with the value from ref. 28. The inset panel of (b) shows the mass, strain and total fluctuation parameters. Solid lines are calculated based on Eqn. (3)-(9). Error bars were added indicating 5% uncertainty in measurements.

Fig. 10 shows the temperature dependence of *ZT* for pristine SnSe, $SnSe_{0.8}Te_{0.2}$ and Na-doped $Sn_{0.99}Na_{0.01}Se_{1-x}Te_x$. It is seen that Te-substitution contributed little enhancement to *ZT* despite a large reduction in thermal conductivity. By doping with Na, *ZT* was enhanced in the whole temperature range, yielding a maximum value of 0.72 at the composition $Sn_{0.99}Na_{0.01}Se_{0.84}Te_{0.16}$ at a relatively low temperature of 773 K. The improvement in thermoelectric performance benefited mainly from the enhanced electrical conductivity by doping with Na. It is also seen that *ZT* values in this work are comparable to or higher than those of polycrystalline samples in previous studies[14,15] in the range of 300-773 K.

Great efforts are still needed to further enhance *ZT* (both the maximum and average values) of polycrystalline SnSe to make it a competitive candidate for possible use in power generation. As currently envisaged, it is crucial to find a dopant to effectively optimize the carrier concentration without deteriorating samples' stability upon heating and cooling cycles; furthermore, band engineering strategies are required to yield a large thermal power while maintaining a high electrical conductivity by virtue of band convergence and/or multi-valley effect; in addition, there is still much room for the reduction of thermal conductivity in polycrystalline SnSe *via* multiscale manipulation of phonon scattering.

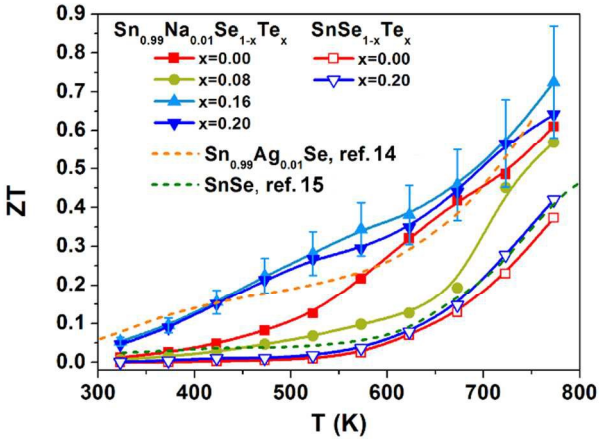

Fig. 10 *ZT* as a function of temperature for pristine and Na-doped $SnSe_{1-x}Te_x$ together with the data for polycrystalline p-type SnSe in ref. 14 and 15. Error bars were added representing 20% uncertainty.

4. Conclusions

In summary, thermoelectric properties of pristine and Na-doped $SnSe_{1-x}Te_x$ polycrystalline alloys were studied. $SnSe_{1-x}Te_x$ solid solutions were formed in the range of x=0-0.2. An energy barrier scattering mechanism was proposed in charge transport of polycrystalline SnSe in association with crystal defects at grain boundaries. The thermal conductivity at room temperature was decreased from 1.4 W/mK for SnSe to 0.8 W/mK for $SnSe_{0.8}Te_{0.2}$, which was mainly ascribed to strain field fluctuations due to Te substitution as well captured by Debye model. By doping with Na, the carrier concentration was increased from ~7×10^{17} to ~1×10^{19} cm^{-3}, leading to the maximum *ZT* = 0.72 for $Sn_{0.99}Na_{0.01}Se_{0.84}Te_{0.16}$ at 773 K. The findings and analyses in this work will help understand thermoelectric transport properties of SnSe and similar chalcogenides as well as their solid solutions.

Acknowledgements

This work is supported by National Natural Science Foundation (Nos. 51172121, 11474176) and the 973 Program (Grant No. 2013CB632503) of China.

Notes and references

**State Key Laboratory of New Ceramics and Fine Processing, School of Materials Science and Engineering, Tsinghua University, Beijing 100084, China. E-mail: jingfeng@mail.tsinghua.edu.cn; Fax: +86-62771160; Tel: +86-10-62784845.*

†Electronic Supplementary Information (ESI) available: XRD patterns of SnSe bulk in two different directions, and DSC patterns for SnSe and $SnSe_{0.8}Te_{0.2}$.

1 L. E. Bell, *Science*, 2008, **321**, 1457-1461.
2 G. J. Snyder and E. S. Toberer, *Nat. Mater.*, 2008, **7**, 105-114.
3 M. G. Kanatzidis, *Chem. Mater.*, 2010, **22**, 648-659.
4 J.-F. Li, W.-S. Liu, L.-D. Zhao and M. Zhou, *NPG Asia Mater.*, 2010,

2, 152-158.
5 X. Zhang and L.-D. Zhao, *Journal of Materiomics*, 2015, **1**, 92-105.
6 J. He, M. G. Kanatzidis and V. P. Dravid, *Mater. Today*, 2013, **16**, 166-176.
7 J. P. Heremans, V. Jovovic, E. S. Toberer, A. Saramat, K. Kurosaki, A. Charoenphakdee, S. Yamanaka and G. J. Snyder, *Science*, 2008, **321**, 554-557.
8 S. I. Kim, K. H. Lee, H. A. Mun, H. S. Kim, S. W. Hwang, J. W. Roh, D. J. Yang, W. H. Shin, X. S. Li and Y. H. Lee, G. J. Snyder and S. W. Kim, *Science*, 2015, **348**, 109-114.
9 G. S. Nolas, D. T. Morelli and T. M. Tritt, *Annu. Rev. Mater. Sci.*, 1999, **29**, 89-116.
10 T. J. Zhu, C. G. Fu, H. H. Xie, Y. T. Liu and X. B. Zhao, *Adv. Energy Mater.*, 2015, **5**, 1500588.
11 W. Liu, H. S. Kim, S. Chen, Q. Jie, B. Lv, M. Yao, Z. Ren, C. P. Opeil, S. Wilson, C.-W. Chu and Z. Ren, *Proc. Natl. Acad. Sci. U. S. A.*, 2015, **112**, 3269-3274.
12 L.-D. Zhao, S.-H. Lo, Y. Zhang, H. Sun, G. Tan, C. Uher, C. Wolverton, V. P. Dravid and M. G. Kanatzidis, *Nature*, 2014, **508**, 373-377.
13 J. Carrete, N. Mingo and S. Curtarolo, *Appl. Phys. Lett.*, 2014, **105**, 101907.
14 C.-L. Chen, H. Wang, Y.-Y. Chen, T. Day and G. J. Snyder, *J. Mater. Chem. A*, 2014, **2**, 11171-11176.
15 S. Sassi, C. Candolfi, J.-B. Vaney, V. Ohorodniichuk, P. Masschelein, A. Dauscher and B. Lenoir, *Appl. Phys. Lett.*, 2014, **104**, 212105.
16 Q. Zhang, E. K. Chere, J. Sun, F. Cao, K. Dahal, S. Chen, G. Chen and Z. Ren, *Adv. Energy Mater.*, 2015, **5**, 1500360.
17 H. Wang, J. Wang, X. Cao and G. J. Snyder, *J. Mater. Chem. A*, 2014, **2**, 3169-3174.
18 C.-F. Wu, T.-R. Wei and J.-F. Li, *Phys. Chem. Chem. Phys.*, 2015, **17**, 13006-13012.
19 D. M. Rowe, ed., *CRC Handbook of Thermoelectrics*, CRC Press, Boca Raton, 1995.
20 E. J. Skoug, J. D. Cain, D. T. Morelli, M. Kirkham, P. Majsztrik and E. Lara-Curzio, *J. Appl. Phys.*, 2011, **110**, 023501.
21 Y. Pei, H. Wang and G. J. Snyder, *Adv. Mater.*, 2012, **24**, 6125-6135.
22 W. Liu, X. Tan, K. Yin, H. Liu, X. Tang, J. Shi, Q. Zhang and C. Uher, *Phys. Rev. Lett.*, 2012, **108**, 166601.
23 A. A. Volykhov, V. I. Shtanov and L. V. Yashina, *Inorg. Mater.*, 2008, **44**, 345-356.
24 Y.-M. Han, J. Zhao, M. Zhou, X.-X. Jiang, H.-Q. Leng and L.-F. Li, *J. Mater. Chem. A*, 2015, **3**, 4555-4559.
25 M. Zhou, Z. M. Gibbs, H. Wang, Y. Han, C. Xin, L. Li and G. J. Snyder, *Phys. Chem. Chem. Phys.*, 2014, **16**, 20741-20748.
26 G. Tan, L.-D. Zhao, F. Shi, J. W. Doak, S.-H. Lo, H. Sun, C. Wolverton, V. P. Dravid, C. Uher and M. G. Kanatzidis, *J. Am. Chem. Soc.*, 2014, **136**, 7006-7017.
27 S. Chen, K. Cai and W. Zhao, *Physica B: Condens. Matter*, 2012, **407**, 4154-4159.
28 B. R. Ortiz, H. Peng, A. Lopez, P. A. Parilla, S. Lany and E. S. Toberer, *Phys. Chem. Chem. Phys.*, 2015, **17**, 19410-19423.
29 H. Liu and L. L. Y. Chang, *J. Alloys Compd.*, 1992, **185**, 183-190.
30 G. S. Nolas, J. Sharp and H. J. Goldsmid, *Thermoelectrics: Basic Principles and New Materials Developments*, Springer, Berlin, 2001.
31 C. Suryanarayana, *Prog. Mater. Sci.*, 2001, **46**, 1-184.
32 F. Li, J.-F. Li, L.-D. Zhao, K. Xiang, Y. Liu, B.-P. Zhang, Y.-H. Lin, C.-W. Nan and H.-M. Zhu, *Energy Environ. Sci.*, 2012, **5**, 7188-7195.
33 L. P. Hu, T. J. Zhu, X. Q. Yue, X. H. Liu, Y. G. Wang, Z. J. Xu and X. B. Zhao, *Acta Mater.*, 2015, **85**, 270-278.
34 W.-S. Liu, Q. Zhang, Y. Lan, S. Chen, X. Yan, Q. Zhang, H. Wang, D. Wang, G. Chen and Z. Ren, *Adv. Energy Mater.*, 2011, **1**, 577-587.
35 L. P. Hu, T. J. Zhu, X. H. Liu and X. B. Zhao, *Adv. Funct. Mater.*, 2014, **24**, 5211-5218.
36 Y. Pan, T.-R. Wei, C.-F. Wu and J.-F. Li, *J. Mater. Chem. C*, 2015, **3**, 10583-10589.
37 A. F. May and G. J. Snyder, in *Thermoelectrics and Its Energy Harvesting*, ed. D. M. Rowe, CRC Press, Boca Raton, 2012, Chap. 11.
38 K. Seeger, *Semiconductor Physics: An Introduction*, Springer Science & Business Media, Berlin, 2013.
39 Q. Tan, L.-D. Zhao, J.-F. Li, C.-F. Wu, T.-R. Wei, Z.-B. Xing and M. G. Kanatzidis, *J. Mater. Chem. A*, 2014, **2**, 17302-17306.
40 J. Y. W. Seto, *J. Appl. Phys.*, 1975, **46**, 5247.
41 J. Martin, L. Wang, L. Chen and G. Nolas, *Phys. Rev. B: Condens. Matter Mater. Phys.*, 2009, **79**, 115311.
42 Y. Zheng, S. Wang, W. Liu, Z. Yin, H. Li, X. Tang and C. Uher, *J. Phys. D: Appl. Phys.*, 2014, **47**, 115303.
43 J. de Boor, T. Dasgupta, H. Kolb, C. Compere, K. Kelm and E. Mueller, *Acta Mater.*, 2014, **77**, 68-75.
44 E. O. Kane, *J. Phys. Chem. Solids*, 1957, **1**, 249-261.
45 H. Wang, Y. Pei, A. D. LaLonde and G. J. Snyder, in *Thermoelectric Nanomaterials: Materials Design and Applications*, eds. K. Koumoto and T. Mori, Springer, Heidelberg, 2013, pp. 3-32.
46 K. W. Schlichting, N. P. Padture and P. G. Klemens, *J. Mater. Sci.*, 2001, **36**, 3003-3010.
47 R. Berman, *Thermal Conduction in Solids*, Clarendon Press, Oxford, 1976.
48 J. Yang, in *Thermal Conductivity: Theory, Properties and Applications*, ed. T. M. Tritt, Plenum, New York, 2004, pp. 1-20.
49 G. A. Slack, *Solid State Physics*, 1979, **34**, 1-71.
50 X. He, H. Shen, W. Wang, Z. Wang, B. Zhang and X. Li, *J. Alloys Compd.*, 2013, **556**, 86-93.
51 H. Wiedemeier, G. Pultz, U. Gaur and B. Wunderlich, *Thermochim. Acta*, 1981, **43**, 297-303.
52 O. Madelung, *Semiconductors-Basic Data*, Springer, Berlin, 1996.
53 J. Callaway, *Phys. Rev.*, 1959, **113**, 1046-1051.
54 G. A. Slack and S. Galginaitis, *Phys. Rev.*, 1964, **133**, A253-A268.
55 P. G. Klemens, *Phys. Rev.*, 1960, **119**, 507-509.
56 J. Yang, G. P. Meisner and L. Chen, *Appl. Phys. Lett.*, 2004, **85**, 1140.
57 R. D. Shannon, *Acta Crystallogr. Sect. A: Cryst. Phys., Diffr., Theor. Gen. Crystallogr.*, 1976, **32**, 751-767.
58 B. Abeles, *Phys. Rev.*, 1963, **131**, 1906-1911.

